Origin and sedimentary evolution of sinkholes (buracas) in the Abrolhos continental shelf, Brazil

Alex C. Bastos [a], Gilberto M. Amado-Filho [b], Rodrigo L. Moura [c], Frederico M. Sampaio [b], Davide Bassi [d], Juan C. Braga [e,]

[a] Departamento de Oceanografia, Universidade Federal do Espírito Santo, Avenida Fernando Ferrari 514, Vitória, ES29090-600, Brazil
[b] Instituto de Pesquisas Jardim Botânico do Rio de Janeiro, Rua Pacheco Leão 915, Rio de Janeiro, RJ22460-030, Brazil
[c] Departamento de Biologia Marinha, Instituto de Biologia, Centro de Ciências da Saúde, Universidade Federal do Rio de Janeiro, Ilhado Fundão, CP68011, Rio de Janeiro, RJ21944-970, Brazil
[d] Dipartimento di Fisica e Scienze della Terra, Università degli Studi di Ferrara, via Saragat 1, I-44122 Ferrara, Italy
[e] Departamento de Estratigrafía y Paleontología, Universidad de Granada, Campus Fuentenueva s/n, 18002 Granada, Spain

Cup-shaped depressions (termed buracas by local fishermen) are common geomorphic features on the north-eastern Abrolhos continental shelf (Brazil). Samples collected by technical diving from the walls of two depres-sions (Buraca Funda, B1, top at 59 m, and Buraca Rasa, B2, top at 26 m) and seismic profiles provide evidence of the processes leading to their formation. The top of the sedimentary succession consists of two units bounded by erosion unconformities. Unit 1 overlies an erosion surface (MR1) and is older than the radiocarbon dating limit. It is made up of packstone to rudstone accumulated on mid- to outer-shelf paleoenvironments. Voids in the lime-stone are filled by a meteoric cement 29,000 cal yrs BP in B2. It is assumed that Unit 1 formed in the late Pleisto-cene, mainly during MIS 5e. An erosion surface (MR2) carved sinkholes in Unit 1, with karstification taking place while the ACS was emergent during the last glacial period. The timing and span of subaerial exposure changes with depth within the shelf. Unit 2 accumulated on this karst surface in the Holocene, after postglacial sea level rise. At the B1 margin, Unit 2 consists of early-lithified packstone to rudstone with attached corals. In B2, the Holocene unit comprises a boundstone of encrusting invertebrates and calcareous algae similar to the living ones attached to the wall today. High productivity in the sinkholes probably promoted the growth of encrusting suspension feeders but also led to intense, multistory bioperforation of carbonates on the wall. The cup-shaped depressions are, therefore, the result of sinkhole formation during the last-glacial low sea levels and later carbon-ate accretion at sinkhole margins during the Holocene

1. Introduction

The Abrolhos continental shelf (ACS) encloses the richest and largest coral-reef system in the South Atlantic (Moura et al., 2013). It covers 46,000 km^2 between the south of Bahia state and the north of Espírito Santo state (Fig. 1). The ACS comprises a mosaic of ecosystems with high endemism, composed of shallow reefs, seagrass and algal meadows, unconsolidated sediments, and the largest rhodolith beds in the world (Amado-Filho et al., 2012; Moura et al., 2013; Bastos et al., 2013). The geomorphology and sedimentology of the ACS, from 25 m depth to the slope, has been characterized since 2007 through acoustic and video images, bottom sampling through diving and remotely oper-ated vehicle, and the acquisition of seismic data (Bastos et al., 2013; Moura et al., 2013; D'Agostini et al., 2015).

Studies on the ACS show that spatial distribution of main habi-tats is related to prior geomorphic evolution due to sea-level oscil-lations during the Quaternary (Vicalvi et al., 1978; Leão and Ginsburg, 1997; Leão and Kikuchi, 1999; Moura et al., 2013; D'Agostini et al., 2015). The record of sea-level oscillations is stored in the mixed siliciclastic-carbonate sediments that make up this platform's Quaternary stratigraphic sequences (Bastos et al., 2013; D'Agostini et al., 2015).

The geomorphic diversity of the Abrolhos shelf includes shallow reefs, pinnacles, mesophotic reefs, paleochannels, and thirty-six struc-tures termed buracas by local fishermen (Bastos et al., 2013; Moura et al., 2013; Fig. 1). Buracas are cup-shaped depressions in a consolidated carbonate substrate, and are known as hotspots of primary productivity and fishing (Land et al., 1995; Cavalcanti et al., 2013).

Cup-shaped depressions in the seafloor can be pockmarks caused by fluids flowing out from the sediment pile or sinkholes of karstic origin (Michaud et al., 2005; Betzler et al., 2011; Kan et al., 2015). Bastos et al. (2013) described these structures, mainly based on geophysical as-sessments, and suggested two hypotheses for their origin. One hypothesis considers the buracas formed by karst processes during sea-level lowstands associated with later, very low sedimentation rates. Ac-cordingly, buracas would be expected to have formed during the Last Glacial Maximum (LGM, late Pleistocene MIS 2) or during earlier lowstand periods (middle Pleistocene MIS 6, MIS 8, etc.). The second hy-pothesis was that the buracas are, partially, a carbonate accretionary feature on top of sinkhole topography. Thus, recent sedimentation on these structures would be represented by granular carbonate sediments or biogenic incrustation on the wall (Bastos et al., 2013). In the latter case, the buracas would record the drowning of the ACS during the post-glacial transgression, and thereby, help to understand the platform's paleoenvironmental evolution.

The lithofacies and components of samples collected directly from the buraca walls were analysed in detail and successive phases of car-bonate sedimentation were radiocarbon dated. The aims of this paper are to: (1) describe the lithofacies and chronostratigraphy of the buraca depressions; (2) discuss the sources of bias in radiometric dating of rocks on exposed submarine walls; and (3) show that the bizarre cup-shaped buracas are a product of erosional karstic processes and the ac-cretion of carbonate sediments promoted by the high productivity char-acteristic of submarine sinkhole-shaped depressions.

2. Material and methods

Two buracas were selected for this study (Fig. 1) based on distance from the coast and depth (Table 1). The Buraca Funda (Deep Buraca, B1) is part of a group of buracas at intermediate depths in the ACS (tops at 50 to 70 m), and the Buraca Rasa (Shallow Buraca, B2) belongs to a group of buracas at relatively shallow depths (tops at 25 to 40 m). In March 2012 the buraca walls were logged through TRIMIX technical diving. In the section logged in B1, 4 carbonate samples were collected at 80 m, 77 m and 65 m (2 samples). In the B2 section 5 samples were taken at 42 m, 40 m, 38 m (2 samples) and 35 m.

A basic macroscopic description of each sample was made with the aid of the hand lens and stereoscopic microscope. From these observa-tions, sample regions were selected for petrographic analysis, and 3 × 3 × 1 cm blocks were cut with the aid of a tungsten handsaw. Nine-teen thin sections were prepared from the nine samples (eight from B1 and eleven from B2) by the National Petrographic Service, Inc. (Hous-ton, Texas, USA).

Thin sections were examined under an Olympus BX43 optical micro-scope with digital camera (Moticam) attached. The images were cap-tured using the Dynamic Scope Image Pro 2009 software. Microfacies analyses of thin sections included carbonate lithofacies identification and skeletal component logging. Fossil components (marine macroin-vertebrates, foraminifers, calcareous algae, and bioperforations) were identified to the most precise taxonomic level possible based on the lit-erature (Tables 2 and 3). Small pieces of selected microfacies and ce-ments were examined under a FEI Quanta-400 ESEM at the Centre for Scientific Instruments (University of Granada, Spain). Polished sections coated by evaporated carbon have been

used to distinguish carbonate fabrics and to obtain their relative elemental composition at selected points. The compositional images were acquired by a solid state backscattered detector and point microanalyses were done by an EDAX Sapphire Si(Li) energy dispersive detector with SUTW. Micro-analysis accuracy is about Â ± 2% using oxide and carbonate standards corrected for microscope geometry and settings. The analyses have been performed at an acceleration voltage of 20 KV and working dis-tance of 10 mm.

Bulk-rock samples (1 cm^3) and selectively drilled subsamples of spe-cific microfacies and cements were analysed for radiocarbon dating at the Center of Applied Isotope Studies (Athens, Georgia, USA) with accel-erator mass spectrometry (AMS). Results were derived from reduction of sample carbon after acid etch pre-treatment to graphite (100% C) with subsequent detection in AMS. Dates are reported as calendar years BP ("present" = 1950 CE) using the 2 sigma confidence interval (Table 4). Calibration was carried out using Calib 7.1 available at http://calib.qub.ac.uk/calib. The Marine13 calibration curve was applied assuming a global marine reservoir effect of 400 years and a Delta R of 85 ± 25 (the average value of the two closest localities) for regional correction.

3. Results

3.1. Lithology and lithofacies

3.1.1. Buraca Funda (B1)

The sampled section, 28 m thick, consists of limestone beds forming ledges with karstic features at the surface (Fig. 2A). The buraca top has a funnel morphology with the surface dipping to the centre and covered by bioclastic sediment with rhodoliths (Fig. 2B). The lower part of the section (from ca. 90 to 76 m) comprises horizontal beds of whitish to greyish limestone with conspicuous borings and dissolution cavities. The limestone consists of coarse-grained packstone to rudstone affected by successive phases of boring and boring filling (Table 2). Serpulids, bryozoans, bivalves, gastropods, echinoderms, ascidian spicules, benthic foraminifers, green calcareous algae and crustose coralline algae (CCA) are the main components of the primary rock (Fig. 2C, D), and also occur in the boring fills together with sponge spicules (Table 2). A drusy, non-luminescent in cathodoluminiscence, iron-free calcite ce-ment partially fills in intraskeletal voids (Fig. 2C, D). Radiaxial fibrous calcite and, locally, botryoidal cements can also be observed (Table 2).

Surface cavities are lined by a thin orange coating encrusted by serpulids, bryozoans, solitary corals, and foraminifers. The outer surface is partially covered by small patches of thin coralline algae.

The upper part of the section consists of whitish bioeroded lime-stone beds gently dipping to the depression centre (Fig. 2A, B). They comprise medium-grained packstone with two successive phases of borings filled by finer-grained packstone (Table 2). Bryozoans, bivalves, benthic foraminifers and coralline algae are the main components in the primary rock. Ascidian and sponge spicules are common in the boring fills (Table 2). Only radiaxial fibrous calcite cement occurs in intraskeletal and intergranular voids.

Most of the exposed surface is encrusted by living crustose and artic-ulated coralline algae (Jania), Peyssonneliacean red algae, serpulids and encrusting foraminifers. A large colony of Montastrea cavernosa was ob-served attached to a bed surface at 65 m.

3.1.2. Buraca Rasa (B2)

In the sampled section at the buraca wall (7 m in thickness), lime-stone beds form ledges with strong dissolution features (Fig. 3A). The base of the upper bed is a notch partially enclosed by an overhanging top (Fig. 3B). The lowest 2 m of the section grainstone filling boring cavities. Pervasive open borings widened by dissolution affect the primary rock and previous bioerosion features. Large coral fragments, fragments of serpulids, corals, echinoderms, bi-valves, gastropods, benthic foraminifers, and red and green calcareous algae are the main components both in the primary rock (Fig. 3C) and boring fills, which also contain ascidian and sponge spicules (Table 3). Intergranular and intraskeletal voids are partially filled by a drusy, non-luminiscent in cathodoluminiscence, non-ferroan calcite cement (Fig. 3C). Clusters and single specimens of brachiopods are attached to cavity surfaces locally showing an orange coating. The outer surface is encrusted by serpulids, small oysters, and foraminifers. Some Gastrochaenolites borings are occupied by bivalves.

A horizontal bed of wackestone to packstone crops out at 40 m. The primary rock and two successive phases of filled borings (Fig. 3D) are af-fected by open borings. Corals fragments (Fig. 3D), echinoderms, ostra-cods, bivalves, ascidian spicules, benthic foraminifers and red and green calcareous algae are the main components of the primary rock, whereas serpulid fragments and sponge spicules are also common in the boring fills (Table 3). Only radiaxial cements can be observed.

The upper beds (from 38 to 35 m) dip to the centre of the depression. They consist of whitish boundstone with packstone matrix, affected by two phases of borings filled by mudstone to grainstone. A last phase of open borings cuts the primary boundstone/packstone and previous bioerosion phases. The boundstone is a complex intergrowth of corals, serpulids, bryozoans, vermetids, bivalves, encrusting foraminifers, and
consist of horizontal beds of greyish rudstone to packstone with a whitish medium-grained coralline algae in varying amounts (Fig. 3E, Table 3). The packstone in-cludes fragments of echinoderms, bivalves, sponge and ascidian spicules (Fig. 3F), benthic foraminifers, Halimeda and coralline algae (Fig. 3F, Table 3). Similar components appear in the boring fills (Fig. 3F, Table 3). Only radiaxial cements can be observed in the samples. The bed sur-face is encrusted by corals, serpulids, small oysters, Spondylus sp., vermetids, branching bryozoans, and foraminifers (including Homotrematids), brachiopods, and warty coralline algae.

3.2. Radiocarbon dating

Radiometric dating of the carbonate samples yielded Late Pleisto-cene to Holocene ages, ranging from 39,200 to 980 cal yrs BP (Table 4). Not all these results, however, can be accepted as valid ages of the target deposit (see Discussion below).

4. Discussion

4.1. Radiocarbon ages and chronostratigraphy

At first sight, the ages underlined in dark grey in Table 4 are inconsis-tent with the marine nature of the dated deposit in its location in the ACS. This shelf is tectonically stable with no significant vertical move-ments during the Holocene (Angulo et al., 2006). Any potential vertical movement during post-LGM shelf reflooding would likely have been slow subsidence due to ocean loading (Mitrovica and Milne, 2002). Tak-ing this into account, the

ages in grey are incompatible with the coeval sea level (Fig. 4), which was several tens of metres below 42 m from 39,200 ± 140 to 17,730 ± 40 yrs ago (Fairbanks, 1989; Lambeck and Chappell, 2001; Grant et al., 2012; Rohling et al., 2014; Lambeck et al., 2014), which are the end values bracketing all ages obtained for bulk rock and primary rock in samples from that depth in B2 (Table 4). Sim-ilarly, sea level was below 80 m from 21,533 ± 500 to 15,243 ± 100 yrs ago (Fairbanks, 1989; Yokoyama and Esat, 2011; Deschamps et al., 2012; Camoin et al., 2012; Lambeck et al., 2014), invalidating the ages obtained within this range for the bulk-rock and primary-rock samples at 77 and 80 m in B1 (Fig. 4). The datings of 12,780 ± 30 cal yrs BP for the bulk rock at 77 m and 13,250 ± 30 cal yrs BP for the bulk rock at 80 m could be compatible with sea level in those ages, but they are in-consistent with other ages yielded by the same hand samples (21,533 ± 500 and 15,243 ± 100 cal yrs BP, respectively). All samples with inconsistent ages contain drusy calcite cements (Figs. 2A, B, 3C) of meteoric origin (see below) formed at about 29,000 cal yrs BP. We as-sume that the primary rock in samples with inconsistent ages (from 42, 77, and 80 m) is older than the radiocarbon dating limit and we consider the obtained inconsistent ages the result of mixing material from the primary rock with much younger deposits due to pervasive boring and fill of bioperforations and void infilling by younger cements. Even when selective drilling of the primary rock was attempted, contamina-tion by younger carbonate, especially cement, could not be avoided.

The age of the selectively drilled primary rock from 40 m at B2, 10,220 ± 30 cal yrs BP is at the very limit of consistency with the ice-volume equivalent sea level proposed by Lambeck et al. (2014); Fig. 4B) but in full agreement with other sea-level reconstructions, such as the one for the western Atlantic by Toscano and Macintyre (2003); Fig. 4B) and the ones by Grant et al. (2012) and Rohling et al. (2014); Fig. 4A). The absence of meteoric cement supports a post-LGM age of the sample, which never experienced emersion.

On the other hand, there is no reason to assume that the bulk-rock ages consistent with coeval sea-level position are true ages of the prima-ry rock since pervasive bioturbation could cause contamination by younger carbonate. The values for one of the bulk-rock samples and the selectively drilled primary rock from 40 m coincide (10,248 ± 30 and 10,220 ± 30 cal yrs BP, respectively) and, therefore, this bulk-rock age can be considered valid. However, another bulk-rock sample from the same depth yielded younger ages (8920 ± 30 cal yrs BP). Even the ages of selectively drilled samples from boring fills should be taken with caution. The earlier phases can be bored as well and contaminated by younger carbonate and, most importantly, all fills of any phase can be contaminated by older material since a varying proportion of particles in borings are fragments of the host rock, many of them chips produced by boring sponges. In summary, in such pervasively bioeroded lithofacies, dating results must be considered potentially biased. Ac-cordingly, in the study deposits, the most reliable ages are those obtain-ed in coral skeletons and cements.

Consequently, discarding inconsistent dating results, two strati-graphic units can be distinguished. Unit 1 comprises the limestone suc-cession older than the radiocarbon dating limit. In B1, it spans from the bottom (93 m) to at least 76 m and in B2 it includes the limestone below 40 m down to the bottom of the sinkhole. Unit 2 is Holocene and in-cludes the top of the wall (from 76 m upwards) in B1 and the beds from 40 m upwards in B2. The limestone beds in Unit 1 contain drusy, non-luminescent, iron-free cement (Figs. 2A, B, 3C) of clear meteoric or-igin (Vollbrecht, 1990; Flügel, 2010). This kind of cement in B2 (Fig. 3C) is about 29,000 cal yrs BP, indicating that limestones in Unit 1 were sub-aerially exposed during the late MIS 3 and MIS 2.

There are no direct chronostratigraphic data of sub-Holocene units at the top of ACS sedimentary pile and no precise age can be assigned to Unit 1 with complete confidence. The few available data, however, suggest a last interglacial (LIG) age for these deposits. Martin et al. (1983) dated a coral sample in an exposed marine terrace in Olivença (Bahia State), around 300 km north of the ACS area. Five coral samples yielded an average U/Th age of 123.5 ± 5.7 ka (Martin et al., 1983), cor-responding to MIS 5e peak of the LIG. As there is no reason to assume a lack of sedimentation on the ACS coeval with the exposed marine ter-race during the LIG inundation of the area, Unit 1 probably formed dur-ing MIS 5. An older age for Unit 1 (i.e., a MIS 7 or older interglacial age) is unlikely as only one phase of dissolution and meteoric cement filling can be observed. As stated above, this cement is 29,000 yrs old suggest-ing that Unit 1 was subaerially exposed only during the last glacial and discarding exposure during MIS 6 or older sea level lowstands. By con-trast, marine sedimentation in the B1 area during the early MIS 3 at about 50,000 yrs ago cannot be excluded according to the sea-level curve proposed by Grant et al. (2012) and Rohling et al. (2014); Fig. 4A). Combining seismic profiles with ages obtained for reefs in the inner arc by Leão and Ginsburg (1997) and Leão et al. (2003), D'Agostini et al. (2015) interpret the major unconformity S1 as an expo-sure surface underlying the Holocene sediments in the coastal area of the ACS and attribute the underlying strata to the Late Pleistocene.

Based on this stratigraphic scheme, the major reflector below the bottom of the depressions in the seismic sections across the buracas (Bastos et al., 2013; MR1 in Fig. 5A, B) must represent a highly irregular erosion surface underlying Unit 1 (Fig. 5A, B), and thus probably corre-sponds to shelf exposure and karstification during the MIS 6 lowstand (Rohling et al., 2014). The reflector that separates Unit 1 from Unit 2 (MR2 in Fig. 5A, B) is an erosion surface carving Unit 1 and producing the buraca depressions during sea-level lowstand and shelf exposure in the late MIS 3 and MIS 2 (Rohling et al., 2014). This reflector corre-sponds to the S1 unconformity of D'Agostini et al. (2015), separating the Pleistocene and Holocene sequences in the inner ACS.

4.2. Paleoenvironmental interpretation

4.2.1. Unit 1

The coarse-grained packstone to rudstone rich in coralline algae comprising the primary rock of Unit 1 in B1 (Fig. 2C) is similar to the modern granular carbonate sediment on the middle to outer shelf in the ACS. The larger porcellaneous foraminifer Archaias (Fig. 2C) and miliolids are common components in inter-reef sediments in the exter-nal reef belt in the modern ACS (Araújo and Machado, 2008). In the Ca-ribbean, Archaias is a eurytopic foraminifer living preferentially in low-energy areas, from lagoons to outer-shelf regions (Cottey and Hallock, 1988), but it is also found in high-energy sediments due to its resistant test (Martin, 1986). The mean annual water temperature optimum for the living species Archaias angulatus ranges from 24 °C to 29 °C (Weinmann et al., 2013). Another common component of Unit 1, the larger benthic foraminifer Amphistegina, is mainly found in the carbon-ate sediments around the Abrolhos external reefs (Araújo and Machado, 2008). Among the algal components, living dasycladales (Neomeris) have been recorded at water depths of several tens of metres whereas Halimeda has a wide depth range and can live below 70 m (Brasileiro et al., 2016), to as deep as 160 m (Bandeira-Pedrosa et al., 2004). Living CCA occur across the Abrolhos shelf to depths below 70 m and the iden-tified articulated corallines (Amphiroa and Jania) can be found below 50 m (Brasileiro et al., 2016). All these packstone components, however, were probably displaced from their original habitats.

The rudstone to packstone in B2 is rich in zooxanthellate coral frag-ments (Fig. 3C), some encrusted by Porolithon onkodes and Titanoderma. P. onkodes inhabits shallow water in the Abrolhos reefs (as Porolithon pachydermum, Figueiredo and Steneck, 2000) and is a dominant species of shallow-water CCA assemblages in less than 10 m in the Indo-Pacific, although it can be found in deeper settings down to 20 m (Adey, 1986; Cabioch et al., 1999; Webster et al., 2009). Titanoderma has a wider depth range and has been recorded in this region at depths of several tens of metres (Brasileiro et

al., 2016). Although these and other compo-nents of the rudstone to packstone have been transported from their habitat, they point to a depositional setting in shallow water close to coral reefs.

4.2.2. Unit 2

The oldest post-LGM sediments are recorded at 40 m depth in B2. They probably formed in very shallow water since global sea-level curves and the ones proposed for the western Atlantic (although show-ing substantial differences for the earliest Holocene) indicate sea level at 25 to −40 m at about 10,200 yrs ago (Toscano and Macintyre, 2003; Blanchon, 2005; Peltier and Fairbanks, 2006; Lambeck et al., 2014). The components (corals, echinoderms; Fig. 3D) suggest a fully marine envi-ronment, and the muddy wackestone lithofacies (Fig. 3D) indicates a low-energy setting. Low turbulence was probably favored by the sea-floor depression where the wackestone accumulated. Later in the Holo-cene, the top 4 m of the B2 wall was built by a boundstone of encrusting CCA, bryozoans, encrusting foraminifers, corals, serpulids, and cemented gastropods (vermetids) and bivalves (oysters) in varying proportions (Fig. 3E). The spaces between the boundstone were filled in by packstone rich in sponge and ascidian spicules (Fig. 3F), suggesting that individuals of these groups of organisms were attached to the skel-etal components of the boundstone. The initial depth of boundstone for-mation (the lowest boundstone yielded a bulk-rock age of about 8500 to 8100 cal yrs BP) was shallower than the present-day one (38 m) as sea level was lower (Toscano and Macintyre, 2003; Peltier and Fairbanks, 2006; Lambeck et al., 2014). In contrast, during the mid-Holocene highstand the area was several metres deeper than today (Angulo et al., 2006). The paleoenvironmental conditions, however, did not change substantially during boundstone accretion and the formation process probably continues nowadays by the encrusting organisms living at the surface. The top of the boundstone at the wall forms a lid hanging over a notch (Fig. 3B). The boundstone changes laterally upslope of the B1 margin to a rhodolith rudstone with a packstone matrix that covers the flat shelf around the depression (Amado-Filho et al., 2012; Moura et al., 2013; Bastos et al., 2015).

The only analysed Unit 2 deposit in B1 is a packstone at its top mar-gin that yielded a bulk-rock age of about 2700 cal yrs BP. The packstone was probably lithified early, and later colonized by younger (980 cal yrs BP) zooxanthellate corals at the wall. The lithofacies and components of these sediments are similar to modern carbonate deposits on the outer ACS (Bastos et al., 2015).

The sediment filling the borings in the Unit 1 primary rock at 77 m in B1 yielded an age of 11,120 ± 35 to 10,560 ± 40 cal yrs BP. As discussed above, these values may be higher than the true age of the deposit since part of the grains in the bioperforations is fragments of the host rock. In any case, these ages are compatible with coeval global sea level (Lambeck et al., 2014), and the boring fills at both 80 and 77 m reflect colonization of the B1 wall by marine bioeroders after post-LGM inun-dation of that sector of the ACS. In the case of Unit 2, bioperforation and boring filling probably started after packstone lithification at 65 m in B1. In B2, the succession of boring phases probably began after wackestone lithification at 40 m and immediately after boundstone for-mation in the upper part of the wall. Boring continues in the hard car-bonate substrate offered by buraca walls.

Inside the perforations, there were accumulations of skeletal parts of epibionts living on the walls, some planktonic elements, ground frag-ments of the host rock, micritic mud and peloids (Tables 2 and 3). Frag-ments of the host rock can locally be interpreted as boring-sponge chips due to characteristic concavely-facetted sides (Schönberg, 2008). Peloids may be the result of micritization of skeletal or host-rock frag-ments (Riding et al., 1991) or be direct precipitates from microbial activ-ity, mainly heterotrophic bacterial calcification (Heindel et al., 2010, 2012; Riding, 2011a). Peloids typically form in semi-isolated cavities (Chafetz, 1986) and are common in borings, usually as geopetal fills (Webster et al., 2009; Riding, 2011b). Boring fills are the result of com-plex biological activities and the filtering of external sediment through openings and galleries and, consequently, broadly coeval infillings show a wide range of textures and composition. The buracas are produc-tivity hotspots (Cavalcanti et al., 2013; Moura et al., 2013) that favour the growth of suspension-feeding encrusters such as bryozoans, serpulids, vermetids, and bivalves, attached suspension feeders such as ascidians and brachiopods, and microbial mats, all of them contribut-ing to boundstone accretion. High productivity, however, also promotes the proliferation of boring suspension feeders such as bivalves, sponges, and worms that destroy the bioconstructed carbonate and facilitate its dissolution.

4.3. Sedimentary evolution of the northeastern ACS

The late-Quaternary sedimentary evolution of the ACS in the buraca region can be reconstructed combining the available seismic profiles (Bastos et al., 2013), chronostratigraphy, and lithofacies of the deposits exposed on the B1 and B2 walls, and proposed sea-level curves for the last 150 ka. The amplitude and exact timing of sea-level oscillations are controversial (Lambeck and Chappell, 2001; Lea et al., 2002; Siddall et al., 2003; Rabineau et al., 2006; Wright et al., 2009; Dorale et al., 2010; Grant et al., 2012; Rohling et al., 2014), and the use of different curves leads to different scenarios for the paleogeographic evolution of the northeastern ACS. In the interest of clarity in the interpretation, only the most recently proposed sea-level curves have been used, namely, the curves of Grant et al. (2012) and Rohling et al. (2014) for the last 150 ka, and the more detailed ones of Toscano and Macintyre (2003), Angulo et al. (2006), and Lambeck et al. (2014) for the last deglacial phase (Fig. 4).

The major reflector below the base of B1 and B2 (MR1, Fig. 5A, B) is an erosion surface presumably corresponding to subaerial exposure of the buraca area during sea-level below − 100 m in MIS 6, about 140 ka ago (Figs. 4A, 6A). Due to the carbonate nature of emergent rocks, the region was subjected to chemical weathering and the development of karst topography (Kendall and Schlager, 1981). Later sea-level rise led to flooding of the entire ACS during MIS 5e (Figs. 4A, 6B) with sea levels sev-eral metres higher than the present day from 128 to 117 ka ago (Lea et al., 2002; Blanchon et al., 2009). The B2 area was subaerially exposed after MIS 5e, and possibly temporarily re-inundated during MIS 5c (from 110 to 100 ka) and MIS 5a (from 85 to 80 ka), according to the curves of Grant et al. (2012) and Rohling et al. (2014); Fig. 4A). The subaerial ex-posure in a single or several periods is reflected in the erosional surface corresponding to MR2 (Fig. 5A). The B1 area (deeper on the shelf) remained submerged for all of MIS 5 (from 128 ka to 80 ka ago) but could have been exposed and re-flooded several times during MIS 4 and the early MIS 3 (according to the curve of Rohling et al., 2014; Fig. 4A). As in the case of B2, the exposure is recorded as the erosional surface of MR2 (Fig. 5B). Facies in Unit 1 indicate a shallow-water depositional setting in the area of B2 and a deeper intermediate- to outer-shelf setting in the area of B1, but the available data do not reveal whether the forma-tion of Unit 1 took place in one or more periods of shelf inundation.

After MIS 5 in the case of B2 and eventually at the end of MIS 3 in the B1 area, sea level fall exposed the northeastern ACS to subaerial karstification and sinkhole formation (Figs. 4A, 6C), which lasted until shelf reflooding due to post-LGM sea-level rise (Figs. 4B, 6D). Subaerial exposure of the inner ACS during the last glacial low sea level is record-ed by an unconformity surface underlying the Holocene sequence (S1 surface of D'Agostini et al., 2015). The B1 area was probably submerged again by 13,500 yrs ago (Bard et al., 2010; Deschamps et al., 2012; Lambeck et al., 2014; Fig. 4B), and a marine environment is first record-ed by boring fills yielding an age of 11,100

yrs ago. According to the global sea-level curve of Lambeck et al. (2014) the B2 area at 40 m depth was re-flooded at about 10,200 cal yrs BP. Bulk rock and selective-ly drilled primary rock ages from this depth (from 8920 ± 30 to 10,250 ± 30 cal yrs BP) are compatible with this inundation timing. The northeastern ACS has been submerged since then while sea level rose to the mid-Holocene peak and then descended several metres (Angulo et al., 2006; Fig. 4B). Vicalvi et al. (1978) analysed the foramin-ifer distribution in a sedimentary core to track the postglacial flooding of the southern ACS. Their results indicate that at 9831 ± 800 cal years BP an estuarine sedimentation dominated the shelf in the so-called Abrolhos depression, which is located at water depths around 50– 55 m. These authors also suggested that full marine conditions started at around 8200 yrs BP, but provided no C14 ages. According to Leão and Ginsburg (1997) and Leão et al. (2003), reef growth re-started in the inner ACS around 7 ka BP, on top of a pre-Holocene reef high. Ac-cording to our estimate, the corrected calendar age for Leão and Ginsburg (1997) coral sample is 5069 ± 300 cal yrs BP.

During the Holocene, sediment accretion around the karstic sink-holes increased the height of the walls by several metres and led to the present-day configuration of these geomorphic features (Fig. 6D). Accretion at the wall was favored by the proliferation of encrusting or-ganisms, which formed a boundstone in B2. In B1, early sediment lithi-fication and attachment of encrusting organisms is the only recorded process promoting wall accretion.

The occurrence of sinkhole-like features in MR1and underlying re-flectors in the seismic profiles of the buraca area (Bastos et al., 2013; Fig. 5B) suggests that the processes of erosion and karstification of the shelf carbonates during low sea level, followed by sediment accumula-tion and buraca wall accretion during rising sea level and highstand took place several times during Pleistocene sea level oscillations.

5. Conclusions

Two cup-shaped depressions (Buraca Funda, B1, top at 59 m, and Buraca Rasa, B2, top at 26 m) were selected to study the origin of these common features in the northeastern Abrolhos continental shelf. Radiocarbon dating, lithofacies, and cements of samples collected by technical diving, as well as available seismic profiles (Bastos et al., 2013), indicate two major sedimentary units separated by erosion sur-faces. The lower unit (Unit 1) overlies a prominent reflector (MR1) and comprises deposits older than the radiocarbon dating limit with intraskeletal and intergranular meteoric cement, which is 29,000 yrs old in B2. Unit 1 is assumed to be late Pleistocene; it most probably formed in MIS 5e although deposition in younger relative sea-level highstands (MIS 5c, MIS 5a, early MIS 3) on the deeper shelf areas (B1 area) cannot be entirely discarded. The top of Unit 1 is bounded by an erosion surface (MR2 reflector) that carved the buraca sinkholes. The upper unit (Unit 2) overlies this surface and is Holocene in age.

Unit 1 comprises packstone to rudstone with fossil components sim-ilar to organisms living on the modern mid and outer ACS. Unit 2 con-sists of early lithified packstone in B1 and boundstone in B2. This boundstone is made of encrusting organisms such as bryozoans, serpulids, vermetid gastropods, bivalves, and encrusting coralline algae and foraminifers, which continue to live on B2 walls. High produc-tivity in the sinkholes probably promoted the growth of the boundstone but also the proliferation of bioeroders and intense boring of the carbon-ate rocks.

The buracas are primarily sinkholes formed during last-glacial low sea level by karstification of the late-Pleistocene Unit 1. The area of the deepest sinkhole (B1) was temporarily exposed after MIS 5 and for a longer period during MIS 2 (i.e., the LGM) whereas intermittent ex-posure of the area of the shallow sinkhole (B2) began after MIS 5e and was continuous from 70 ka until the early Holocene. The upper part of the sinkhole walls (Unit 2), however, is the result of carbonate accretion during the Holocene. Therefore, the buracas are partially carbonate ac-cretionary features formed on top of sinkholes, confirming the second hypothesis of Bastos et al. (2013).

Acknowledgements

Financial support was provided by Brazilian Science and Technology Agency CNPq (563266/2010-4 and 305449/2014-1 projects; research grants for ACB, GMAF and RLM), CAPES (IODP project, Ciências do Mar II/CAPES Grant 23038.004312/2014-74), FAPES (project 54161320/ 2011), and by P&D ANP/BRASOIL project. The work of JCB was funded by the Brazilian Science and Technology Ministry within the Program Science Without Borders, project MCTI/MEC no. 400654/2014-8 “Reconstrução Paleoecológica e Paleoclimática da Plataforma Continen-tal de Abrolhos” (Paleoecological and Paleoclimatic reconstruction of Abrolhos Continental Shelf). We thank Christine Laurin for the revision of the English text. This is a contribution from Rede Abrolhos.

References

Adey, W.H., 1986. Coralline algae as indicators of sea-level. In: van de Plassche, O. (Ed.), Sea-Level Research: A Manual for the Collection and Evaluation of Data. Geo Books, Norwich, pp. 229–279.

Amado-Filho, G.M., Moura, R.L., Bastos, A.C., Salgado, L.T., Sumida, P.Y., Guth, A.Z., Francini-Filho, R.B., Pereira-Filho, G.H., Abrantes, D.P., Brasileiro, P.S., Bahia, R.G., Leal, R.N., Kaufman, L., Kleypas, J.A., Farina, M., Thompson, F.L., 2012. Rhodolith beds are major CaCO3 bio-factories in the tropical south West Atlantic. PLoS One 7 (4), 1–6. http://dx.doi.org/10.1371/journal.pone.0035171.

Angulo, R.J., Lessa, G.C., de Souza, M.C., 2006. A critical review of mid- to late-Holocene sea-level fluctuations on the eastern Brazilian coastline. Quat. Sci. Rev. 25, 486–506. http://dx.doi.org/10.1016/j.quascirev.2005.03.008.

Araújo, H.A.B., Machado, A.J., 2008. Benthic foraminifera associated with the south Bahia coral reefs, Brazil. J. Foraminifer. Res. 38, 23–38.

Bandeira-Pedrosa, M.E., Pereira, S.M.B., Oliveira, E.C., 2004. Taxonomy and distribution of the green algal genus Halimeda (Bryopsidales, Chlorophyta) in Brazil. Rev. Bras. Bot. 27, 363–377.

Bard, E., Hamelin, B., Delanghe-Sabatier, D., 2010. Deglacial meltwater pulse 1B and Youn-ger Dryas sea levels revisited with boreholes at Tahiti. Science 327, 1235–1237.

Bastos, A.C., Moura, R.L., Amado-Filho, G.M., D'Agostini, D.P., Secchin, N.A., Francini-Filho, R.B., Güth, A.Z., Sumida, P.Y.G., Mahiques, M., Thompson, F.L., 2013. Buracas: novel and unusual sinkhole-like features in the Abrolhos Bank. Cont. Shelf Res. 70, 118–125. http://dx.doi.org/10.1016/j.csr.2013.04.035.

Bastos, A.C., Quaresma, V.S., Marangoni, M.B., D'Agostini, D.P., Bourguignon, S.N., Cetto, P.H., Silva, A.E., Amado-Filho, G.M., Moura, R.L., Collins, M., 2015. Shelf morphology as an indicator of sedimentary regimes: a synthesis from a mixed siliciclastic–carbon-ate shelf on the eastern Brazilian margin. J. S. Am. Earth Sci. 63, 125–136. http://dx.doi.org/10.1016/j.jsames.2015.07.003.

Betzler, C., Lindhorst, S., Hübscher, C., Lüdmann, T., Fürstenau, J., Reijmer, J., 2011. Giant pockmarks in a carbonate platform (Maldives, Indian Ocean). Mar. Geol. 289, 1–16. http://dx.doi.org/10.1016/j.margeo.2011.09.004.

Blanchon, P., 2005. Comments on “corrected western Atlantic sea-level curve for the last 11,000 years based on calibrated 14C dates from Acropora palmata framework and in-tertidal mangrove peat” by Toscano and Macintyre. Coral Reefs 24, 183–186.

Blanchon, P., Eisenhauer, A., Fietzke, J., Liebetrau, V., 2009. Rapid sea-level rise and reef back-stepping at the close of the last interglacial highstand. Nature 458, 881–884.

Brasileiro, P.S., Pereira-Filho, G.H., Bahia, R.G., Abrantes, D.P., Guimarães, S.M.P.B., Moura, R.L., Francini-Filho, R.B., Bastos, A.C., Amado-Filho, G.M., 2016. Macroalgal composi-tion and community structure of the largest rhodolith beds in the world. Mar. Biodivers. 46, 407–420. http://dx.doi.org/10.1007/s12526-015-0378-9.

Cabioch, G., Montaggioni, L.F., Faure, G., Ribaud-Laurenti, A., 1999. Reef coralgal assem-blages as recorders of paleobathymetry and sea level changes in the Indo-Pacific province. Quat. Sci. Rev. 18, 1681–1695.

Camoin, G.F., Seard, C., Deschamps, P., Webster, J.M., Abbey, E., Braga, J.C., Iryu, Y., Durand, N., Bard, E., Hamelin, B., Yokoyama, Y., Thomas, A.L., Henderson, G.M., Dussouillez, P., 2012. Reef response to sea-level and environmental changes during the last deglaci-ation: Integrated Ocean Drilling Program Expedition 310, Tahiti sea level. Geology 40, 643–646. http://dx.doi.org/10.1130/G32057.1.

Cavalcanti, G., Gregoracci, G.B., Moura, R.L., Amado-Filho, G., Longo, L.L., Bastos, A.C., Ferreira, C.M., Francini-Filho, R.B., Paranhos, R., Ghisolfi, R.D., Krüger, R., Güth, A.Z., Sumida, P.Y.G., Maia-Neto, O., Santos, E.O., Lida, T., Thompson, F.L., 2013. Sinkholes-like structures as bioproductivity hotspots in the Abrolhos bank. Cont. Shelf Res. 70, 126–134. http://dx.doi.org/10.1016/j.csr.2013.05.011.

Chafetz, H.S., 1986. Marine peloids; a product of bacterially induced precipitation of cal-cite. J. Sediment. Petrol. 56, 812–817.

Cottey, T.L., Hallock, P., 1988. Test surface degradation in Archaias angulatus.
J. Foraminifer. Res. 18, 187–202.

D'Agostini, D.P., Bastos, A.C., dos Reis, A.T., 2015. The modern mixed carbonate–siliciclastic Abrolhos shelf: implications for a mixed depositional model. J. Sediment. Res. 85, 124–139. http://dx.doi.org/10.2110/jsr.2015.08.

Deschamps, P., Durand, N., Bard, E., Hemelin, B., Camoin, G., Thomas, A., Henderson, G.M., Okuno, J., Yokoyama, Y., 2012. Ice-sheet collapse and sea-level rise at the Bolling warming 14.600 years ago. Nature 483, 559–564. http://dx.doi.org/10.1038/ nature10902.

Dorale, J.A., Onac, B.P., Fornós, J.J., Ginés, J., Ginés, A., Tuccimei, P., Peate, D.W., 2010. Sea-level highstand 81.000 years ago in Mallorca. Science 327, 860–863. http://dx.doi.org/10.1126/science.1181725.

Fairbanks, R.G., 1989. A 17,000 year glacio-eustatic sea level record: Influence of glacial melting rates on the Younger Dryas event and deep-ocean circulation. Nature 342, 637–642.

Figueiredo, M.A., Steneck, R., 2000. Floristic and ecological studies of crustose coralline algae on Brazil's Abrolhos reefs. Proceedings 9th International Coral Reef Symposium 1, pp. 493–498.

Flügel, E., 2010. Microfacies of Carbonate Rocks. Springer, Berlin Heidelberg http://dx.doi.
org/10.1007/978-3-662-08726-8.

Grant, K.M., Röhling, E.J., Bar-Matthews, B., Ayalon, A., Medina-Elizalde, M., Ramsey, C.B., Satow, C., Roberts, A.P., 2012. Rapid coupling between ice volume and polar temper-ature over the past 150,000 years. Nature 491, 744–747.

Heindel, K., Birgel, D., Brunner, B., Thiel, V., Westphal, H., Gischler, E., Ziegenbalg, S.B., Cabioch, G., Sjövall, P., Peckmann, J., 2012. Post-glacial microbialite formation in coral reefs in the Pacific, Atlantic, and Indian oceans. Chem. Geol. 304–305, 117–130.

Heindel, K., Birgel, D., Peckmann, J., Kuhnert, H., Westphal, H., 2010. Formation of deglacial microbialites in coral reefs off Tahiti (IODP 310) involving sulfate-reducing bacteria. PALAIOS 25, 618–635.

Kan, H., Urata, K., Nagao, M., Hori, N., Fujita, K., Yokoyama, Y., Nakashima, Y., Ohashi, T., Goto, K., Suzuki, A., 2015. Submerged karst landforms observed by multibeam bathy-metric survey in Nagura Bay, Ishigaki Island, southwestern Japan. Geomorphology 229, 112–124.

Kendall, C.G.S.C., Schlager, W., 1981. Carbonates and relative changes in sea level. Mar.
Geol. 44, 181–212. http://dx.doi.org/10.1016/0025-3227(81)90118-3.

Lambeck, K., Chappell, J., 2001. Sea level change through the last glacial cycle. Science 292, 679–686. http://dx.doi.org/10.1126/science.1059549.

Lambeck, K., Rouby, H., Purcell, A., Sun, Y., Sambridge, M., 2014. Sea level and global ice volumes from the last glacial maximum to the Holocene. Proc. Natl. Acad. Sci. U. S. A. 111 (43), 15296–15303.

Land, L.A., Paull, C.K., Hobson, B., 1995. Genesis of a submarine sinkhole without subaerial exposure: Straits of Florida. Geology 23, 949–951. http://dx.doi.org/10.1130/0091-7613(1995)023b0949:GOASSWN2.3.CO;2.

Lea, W.D., Martin, P.A., Pak, D.K., Spero, H.J., 2002. Reconstructing a 350 ky history of sea level using planktonic Mg/Ca and oxygen isotope records from a Cocos ridge core. Quat. Sci. Rev. 21, 283–293. http://dx.doi.org/10.1016/S0277-3791(01)00081-6.

Leão, Z.M.A.N., Ginsburg, R., 1997. Living reefs surrounded by siliciclastic sediments: the Abrolhos coastal reefs, Bahia, Brazil. In: Lessios, H.A., Macintyre, I.G. (Eds.), Proceed-ings of the 8th International Coral Reef Symposium Vol. 2. Smithsonian Tropical Re-search Institute, Panama, pp. 1767–1772.

Leão, Z.M.A.N., Kikuchi, R.K.P., 1999. The Bahian coral reefs – from 7000 years BP to 2000 years AD. Ciência e Cultura 51, 262–273.

Leão, Z.M.A.N., Kikuchi, R.K.P., Testa, V., 2003. Corals and coral reefs of Brazil. In: Cortés, J.
(Ed.), Latin American Coral Reefs. Elsevier, Amsterdam, pp. 9–52.

Martin, R.E., 1986. Habitat and distribution of the foraminifer Archaias angulatus (Fichtel and Moll) (Miliolina, Soritidae), northern Florida keys. J. Foraminifer. Res. 16, 201–206.

Martin, L., Bittencourt, A.C.S.P., Vilas-Noas, G.S., 1983. Primeira ocorrência de corais pleistocênicos da costa brasileira: Datação do máximo da penúltima transgressão. Ciências da Terra 3, 16–17.

Michaud, F., Chabert, A., Collot, J.Y., Sallare, V., Flueh, E.R., Charvis, P., Graindorge, D., Gustcher, M.A., Bialas, J., 2005. Fields of multi-kilometer scale sub-circular depres-sions in the Carnegie ridge sedimentary blanket: effect of underwater carbonate dis-solution? Mar. Geol. 216, 205–219. http://dx.doi.org/10.1016/j.margeo.2005.01.003.

Mitrovica, J.X., Milne, G.A., 2002. On the origin of late Holocene sea-level highstands with-in equatorial ocean basins. Quat. Sci. Rev. 21, 2179–2190.

Moura, R.L., Secchin, N.A., Amado-Filho, G.M., Francini-Filho, R.B., Freitas, M.O., Minte-Vera, C.V., Teixeira, J.B., Thompson, F.B., Sumida, P.Y.G., Guth, A.Z., Bastos, A.C., 2013. Spatial patterns of benthic megahabitats and conservation planning. Cont. Shelf Res. 70, 109–117. http://dx.doi.org/10.1016/j.csr.2013.04.036.

Peltier, W.R., Fairbanks, R.G., 2006. Global glacial ice volume and last glacial maximum du-ration from an extended Barbados sea level record. Quat. Sci. Rev. 25, 3322–3337.

Rabineau, M., Berné, S., Olivet, J.L., Aslanian, D., Guillocheau, F., Joseph, P., 2006. Paleo sea levels reconsidered from direct observation of paleoshoreline position during glacial maxima (for the last 500.000 yr). Earth Planet. Sci. Lett. 252, 119–137. http://dx.doi. org/10.1016/j.epsl.2006.09.033.

Riding, R., 2011a. Reefal microbial crusts. In: Hopley, D. (Ed.), Encyclopedia of Modern Coral ReefsEncyclopedia of Earth Science Series. Springer, Heidelberg, pp. 911–915.

Riding, R., 2011b. Microbialites, stromatolites, and thrombolites. In: Reitner, J., Thiel, V. (Eds.), Encyclopedia of GeobiologyEncyclopedia of Earth Science Series. Springer, Heidelberg, pp. 635–654.

Riding, R., Martín, J.M., Braga, J.C., 1991. Coral stromatolite reef framework, Upper Mio-cene, Almeria, Spain. Sedimentology 38, 799–818.

Rohling, E.J., Foster, G.L., Grant, K.M., Marino, G., Roberts, A.P., Tamisiea, M.E., Williams, F., 2014. Sea-level and deep-sea-temperature variability over the past 5.3 million years. Nature 508, 477–482.

Schönberg, C.H.L., 2008. A history of sponge erosion: from past myths and hypotheses to recent approaches. In: Wisshak, M., Tapanila, L. (Eds.), Current Developments in BioerosionErlangen Earth Conference Series. Springer-Verlag, Berlin Heidelberg, pp. 165–202 http://dx.doi.org/10.1007/978-3-540-77598-0_9.

Siddall, M., Rohling, E.J., Almogi-Labin, A., Hemleben, C., Meischner, D., Schmeltzer, I., Smeed, D.A., 2003. Sea-level fluctuations during the last glacial cycle. Nature 423, 853–858. http://dx.doi.org/10.1038/nature01690.

Toscano, M., Macintyre, I.G., 2003. Corrected western Atlantic sea-level curve for the last 11,000 years based on calibrated 14C dates from Acropora palmata framework and in-tertidal mangrove peat. Coral Reefs 22, 257–270.

Vicalvi, M.A., Costa, M.P.A., Kowsmann, R.O., 1978. Depressão dos Abrolhos: uma paleolaguna Holocênica na plataforma continental leste brasileira. Boletim Técnico da Petrobrás 21, 279–286.

Vollbrecht, R., 1990. Marine and meteoric diagenesis of submarine Pleistocene carbonates from the Bermuda carbonate platform. Carbonates Evaporites 5, 13–96. http://dx.doi.org/10.1007/BF03174319.

Webster, J.M., Braga, J.C., Clague, D.A., Gallup, C., Hein, J.R., Potts, D.C., Renema, W., Riding, R., Riker-Coleman, K., Silver, E., Wallace, L.M., 2009. Coral reef evolution on rapidly subsiding margins. Glob. Planet. Chang. 66, 129–148.

Weinmann, A.E., Rödder, D., Lötters, S., Langer, M.R., 2013. Heading for new shores: projecting marine distribution ranges of selected larger Foraminifera. PLoS One http://dx.doi.org/10.1371/journal.pone.0062182.

Wright, J.D., Sheridan, R.E., Miller, K.G., Uptegrove, J., Cramer, B.S., Browning, J.V., 2009. Late Pleistocene sea level on the New Jersey margin: implications to eustasy and deep-sea temperature. Glob. Planet. Chang. 66, 93–99. http://dx.doi.org/10.1016/j. gloplacha.2008.03.013.

Yokoyama, Y., Esat, T.M., 2011. Global climate and sea level enduring variability and rapid fluctuations over the past 150,000 years. Oceanography 24, 54–69. http://dx.doi.org/10.5670/oceanog.2011.27.

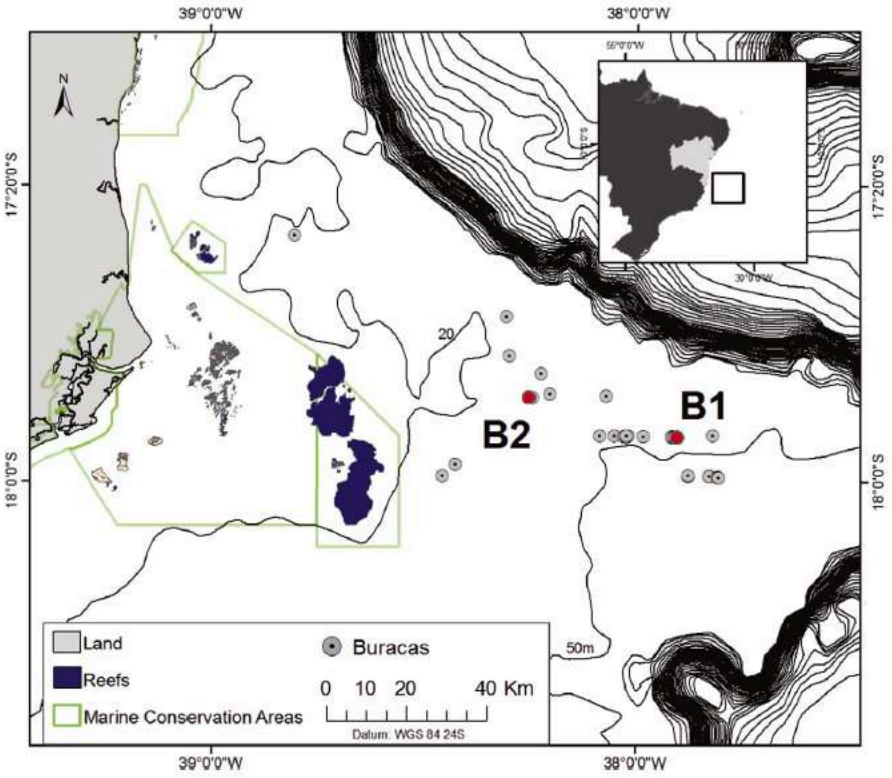

Fig. 1. Location of the *buracas* (grey dots) in the Abrolhos continental shelf. B1and B2 (red dots) are the examples studied.

Table 2
Lithofacies, main components and cements of samples from Buraca Funda (B1). P: primary rock; Bf1 and Bf2: boring filling phases; CCA: crustose coralline algae; ACA: articulated coralline algae; EF: encrusting foraminifers; LBF: larger benthic foraminifers; SBF: small benthic foraminifers; PF: planktonic foraminifers.

Depth	Mesoscopic features	Lithofacies	Main components	Cements
80 m	Whitish limestone with conspicuous pervasive borings (*Gastrochaenolites*, *Entobia*, *Trypanites*), most of them filled in with a grey deposit	P: brownish coarse-grained packstone to rudstone (Fig. 2C)	Corals, serpulids, bryozoans, bivalves, gastropods, echinoderms, ascidian spicules, LBF (*Archaias*, Fig. 2C, *Amphistegina*), SBF, green calcareous algae *Halimeda* and dasycladales, CCA and ACA (*Amphiroa*, *Jania*), Peyssonneliaceans	Drusy calcite in intraskeletal spaces (Fig. 2C); botryoidal cement; radiaxial fibrous calcite
		Bf1: darker brownish, fine- to medium-grained packstone filling borings and voids in the primary rock; locally, foraminifers encrusted the surface of borings	Ascidian spicules, sponge spicules, echinoderms, bivalves, ostracods, SBF, CCA	
		Bf2: grey wackestone to grainstone partially to totally filling borings in P (Fig. 2C) and Bf1	Ascidian spicules, sponge spicules, molluscs, echinoderms, SBF, PF, CCA, packstone fragments (sponge chips) and peloids	
77 m	Greyish limestone with borings filled in by a whitish material	P: brownish medium - to coarse packstone to rudstone	Serpulids, bryozoans, bivalves, gastropods (including vermetids), echinoderms, ascidian spicules, ostracods, LBF (*Archaias*), SBF, *Halimeda*, CCA and ACA	Drusy, non-luminescent in cathodoluminiscence, iron-free cement in intraskeletal voids (Fig. 2D)
		Bf1: darker fine- to medium grained packstone to wackestone filling borings and voids in P	Serpulids, bryozoans, brachiopods, echinoderms, bivalves, gastropods, ascidian spicules, LBF (*Amphistegina*), SBF, *Halimeda*, Peyssonneliaceans, packstone fragments	Radiaxial fibrous in intraskeletal voids
65 m	Whitish limestone with borings filled in by a white deposit	P: medium-grained brownish packstone	Bryozoans, bivalves, LBF (*Amphistegina*), SBF, CCA, ACA	Radiaxial fibrous in intraskeletal and intergranular voids
		Bf1: finer-grained packstone rich in micritic matrix filling borings in P	Ascidian spicules, bivalves, ostracods, SBF, packstone fragments (sponge chips)	
		Bf2: greyish peloidal packstone to grainstone filling borings and voids in P, Bf1 and coral skeleton; Bf2 perforated by open borings containing loose sand-grade bioclasts	Sponge spicules, ascidian spicules, SBF, locally clotted peloids	

Table 3
Lithofacies, main components, and cements of samples from Buraca Rasa (B2). P: primary rock; Bf1 and Bf2: boring filling phases; CCA: crustose coralline algae; ACA: articulated coralline algae; EF: encrusting foraminifers; LBF: larger benthic foraminifers; SBF: small benthic foraminifers; PF: planktonic foraminifers.

Depth	Mesoscopic features	Lithofacies	Main components	Cements
42 m	Greyish limestone with borings filled in by a whitish material, both cut by open borings (*Gastrochaenolites*, *Entobia* and *Trypanites*, and microborings)	P: rudstone to packstone (Fig. 3C)	Large coral fragments, locally encrusted by coralline algae (*Porolithon onkodes* and *Titanoderma*), serpulids and vermetids; fragments of serpulids, corals, echinoderms, bivalves, gastropods, LBF (*Amphistegina*), SBF, EF, *Halimeda*, CCA, ACA (*Amphiroa*)	Drusy, non-luminiscent in cathodoluminiscence, iron-free cement (Fig. 3C) in intergranular and intraskeletal voids
		Bf1: medium-grained grainstone	Serpulids, corals, echinoderms, bivalves, gastropods, ostracods, ascidian spicules, sponge spicules, LBF, SBF, PF, CCA, packstone fragments	Botryoidal in intraskeletal voids; small fibrous crystals
40 m	Greyish limestone with borings filled in by a whitish material, both cut by open borings	P: brownish wackestone to packstone (Fig. 3D)	Large corals fragments, echinoderms, ostracods, bivalves, ascidian spicules, LBF (*Archaias*), SBF, *Halimeda*, ACA	
		Bf1: darker wackestone to packstone filling borings in P (Fig. 3D)	Serpulids, corals, echinoderms, bivalves, vermetids, ascidian spicules, sponge spicules, LBF (*Archaias*), SBF, *Halimeda*, CCA, ACA (*Amphiroa*)	
		Bf2: greyish peloidal mudstone to grainstone partially to totally filling borings in P and Bf1 (Fig. 3D)	Serpulids, brachiopods, ascidian spicules, sponge spicules, SBF, *Halimeda*, ACA, packstone fragments, peloids, locally clotted	
38 m	Whitish limestone with borings filled in by a white deposit, both cut by open borings and dissolution cavities	P: boundstone with packstone matrix	Boundstone: CCA (*Mesophyllum*, *Sporolithon*, *Titanoderma*), bryozoans, corals, serpulids, vermetids, oysters, and EF Packstone: echinoderms, bivalves, ascidian spicules, sponge spicules, LBF (*Archaias*), SBF, EF, *Halimeda*, CCA (*Paulsilvella*, *Lithoporella*), ACA (*Amphiroa*, Corallinoideae)	Radiaxial cement in some pores of wackestone
		Bf1: wackestone filling borings and voids in P	Serpulids, echinoderms, bivalves, vermetids, ascidian spicules, LBF (*Archaias*), SBF, *Halimeda*, CCA (*Paulsilvella*), ACA (*Amphiroa*)	
		Bf2: mudstone to grainstone filling borings and voids in P and Bf1	Echinoderms, ascidian spicules, sponge spicules, molluscs, LBF (*Archaias*, *Amphistegina*), SBF, *Halimeda*, CCA (*Paulsilvella*, Fig. 3F), ACA (*Amphiroa*, Corallinoideae), clotted peloids	
35 m	Whitish limestone with borings filled by a white deposit, both cut by open borings and dissolution cavities. Large coral colonies (*Siderastrea*)	P: boundstone with a packstone matrix (Fig. 3E)	Boundstone: Corals, serpulids, bryozoans, EF, and CCA (*Sporolithon*) Packstone: serpulids, molluscs, ascidian spicules, LBF, SBF, CCA	Radiaxial cement in intraskeletal voids
		Bf1: wackestone filling borings and voids in P	Serpulids, molluscs, ascidian spicules, sponge spicules, LBF, SBF, fragments of packstone	
		Bf2: mudstone to grainstone partially filling borings and voids in P and Bf1	Echinoderms, molluscs, ascidian spicules, sponge spicules, SBF, peloids locally clotted	

Table 4
Calibrated ages of samples from the *buracas* B1 and B2. In dark grey: sample ages inconsistent with their location in the ACS; in light grey: sample ages compatible with sea-level position in their locations but inconsistent with other ages of the same hand samples. Bf1 and Bf2: boring filling phases.

Site	Depth	Sample/Sample nature	2 σ Calibrated years BP
B2 (Buraca Rasa)	35 m	35a/bulk rock	5286 ± 80
		35b/coral	5190 ± 120
	38 m	38a/bulk rock	8461 ± 60
		38b/bulk rock	8165 ± 60
	40 m	40a/bulk rock	8920 ± 30
		40b/bulk rock	10248 ± 30
		40/primary rock	10220 ± 30
		40/Bf1	8830 ± 30
		40/Bf2	6830 ± 30
	42 m	42a/bulk rock	22980 ± 50
		42b/bulk rock	22980 ± 50
		42c/bulk rock	17730 ± 40
		42d/bulk rock	37130 ± 140
		42e/bulk rock	39200 ± 140
		42/primary rock	33470 ± 140
		42/drusy cement 1	29040 ± 100
		42/drusy cement 2	29360 ± 110
B1 (Buraca Funda)	65 m	65a/bulk rock	2749 ± 30
		65b/coral	980 ± 20
	77 m	77a/bulk rock	21533 ± 500
		77b/bulk rock	12780 ± 30
		77/primary rock	15840 ± 50
		77/Bf1	11120 ± 35
		77/Bf1	10560 ± 40
	80 m	80a/bulk rock	15243 ± 100
		80b/bulk rock	13250 ± 30

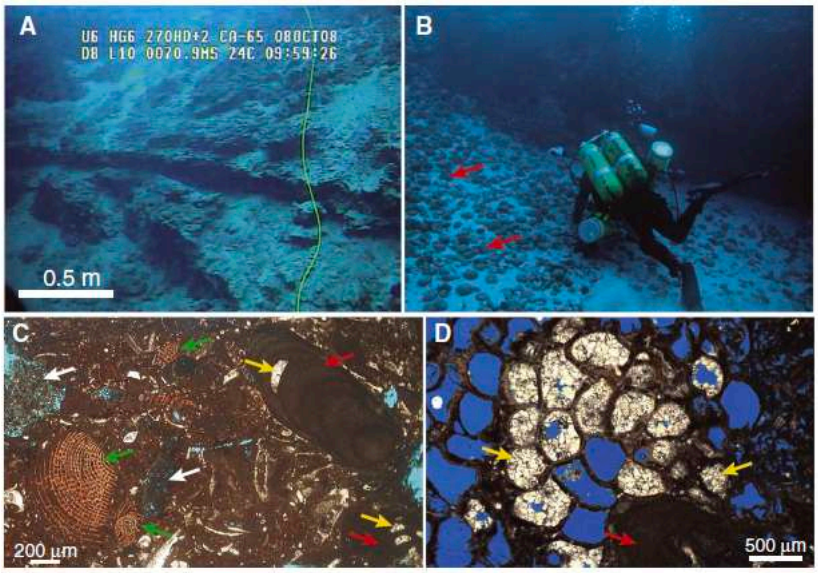

Fig. 2. A) ROV image of the Buraca Funda (B1) wall at about 70 m depth. B) Top of the B1 wall dipping to the *buraca* centre. Note rhodoliths (arrows) on the sediment (bioclastic carbonate sand) surface. C) Micrograph of primary rock (coarse-grained packstone to rudstone) and boring fills (Bf2, white arrows) at 80 m in B1. Coralline algae (red arrows) and the larger benthic porcellaneous foraminifer *Archaias* (green arrows) are main components of the primary rock. The intraskeletal voids (conceptacles) of coralline algae are filled by a drusy cement (yellow arrows). D) Micrograph of coralline algae (red arrow) and bryozoan colony with intraskeletal voids filled by drusy, iron-free calcite cement (yellow arrows). Primary rock at 80 m in B1.

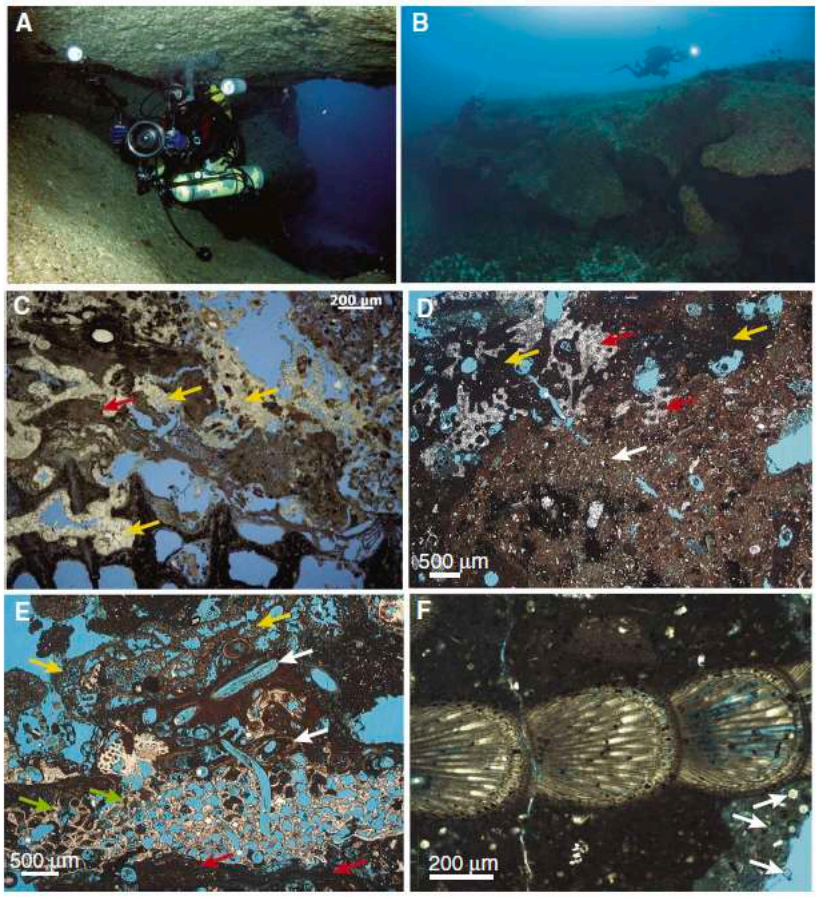

Fig. 3. A) Karstic cavity at the Buraca Rasa (B2) wall at 39 m depth. B) Top of B2 wall at 35 m. Note top bed dipping to the *buraca* centre and notch partially enclosed by an overhanging lid at its base (photo by Athila Bertoncini). C) Rudstone with coral encrusted by coralline algae (red arrow) with intraskeletal and interskeletal drusy calcite cement (yellow arrows). Sample from B2 at 42 m depth. D) Primary wackestone to packstone (white arrows) with coral (red arrows) and darker wackestone (yellow arrows) filling a first phase of borings and intraskeletal spaces at 40 m depth in B2. E) Boundstone of coralline algae (red arrows), bryozoans (green arrows), serpulids (white arrows), and encrusting foraminifers (yellow arrows) from 35 m in B2. F) The coralline alga *Paulsilvella* is common in the boundstone at 38 m in B2. Note the occurrence of ascidian spicules (white arrows).

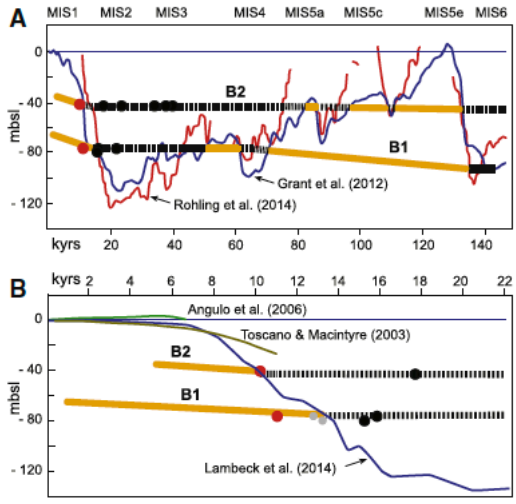

Fig. 4. A) Sea-level reconstructions for the last 150 ka based on the Red Sea (Grant et al., 2012) and Eastern Mediterranean (Rohling et al., 2014) record. B) Ice-volume equivalent sea-level curve for the last 22 ka (Lambeck et al., 2014), and reconstructions for the last 11 ka based on the western Atlantic (Toscano and Macintyre, 2003), and for the last 7 ka based on the eastern Brazilian shelf (Angulo et al., 2006) records. Black circles: age/depth location of inconsistent radiocarbon ages; grey circles: age/depth location of samples compatible with sea-level position, but obtained from the same samples that yielded inconsistent ages; red circles: first marine record after LGM. B1 and B2: sedimentary evolution of the Buraca Funda and Buraca Rasa areas, respectively. Solid orange lines: intervals of inundation and potential deposition; dashed lines: intervals of emersion and karstification; narrow dashes indicate disagreement between proposed sea-level reconstructions; mbsl: metres below sea level; kyrs: thousand years; MIS: marine isotope stage.

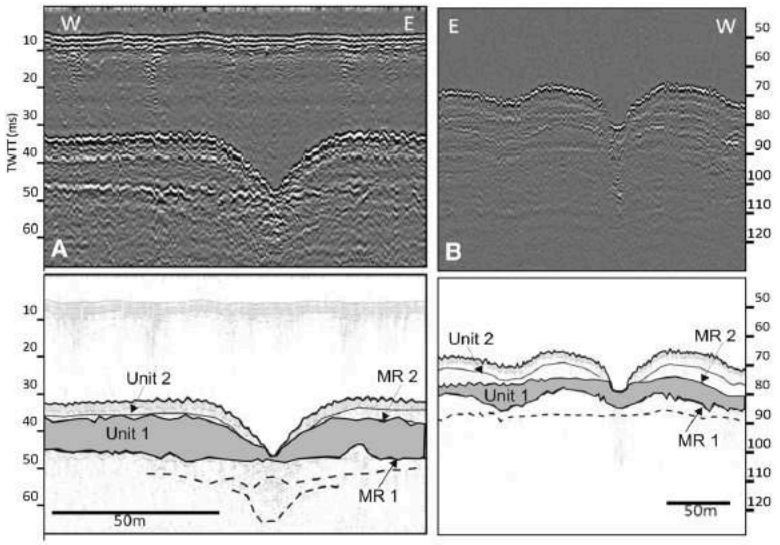

Fig. 5. Stratigraphy of B2 (A) and B1 (B) based on lithology, radiocarbon ages and seismic profiles (Bastos et al., 2013). MR1 and MR2 are major reflectors. TWTT (ms): *two-way travel time* (milliseconds).

V

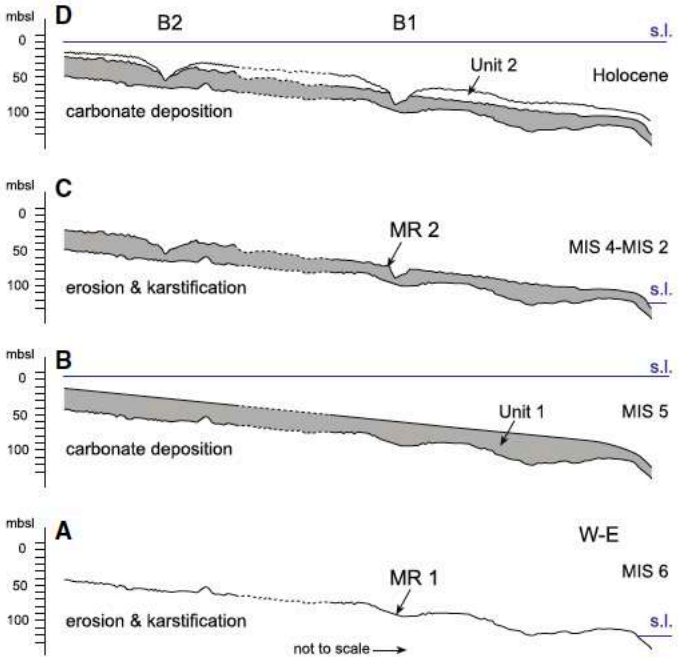

Fig. 6. Simplified sedimentary evolution (A to D) of the northeastern ACS in B1 and B2 areas. mbsl: metres below sea level; MIS: marine isotope stage; MR1 and MR2: major reflectors; s.l: sea level.